



Cite this: *New J. Chem.*, 2019, 43, 18251

## Positive charge-dependent cell targeted staining and DNA detection†

Pei Yin,<sup>a</sup> Tao Wang,<sup>a</sup> Yuan Yang,<sup>a</sup> Weidong Yin,<sup>a</sup> Shaoxiong Zhang,<sup>a</sup> Zengming Yang,<sup>a</sup> Chunxuan Qi<sup>b</sup> and Hengchang Ma<sup>ib</sup>\*<sup>a</sup>

The chemical structures or positive charge-guided specific cell organelles' staining was an interesting but very challenging research work. In this paper, we synthesized a series of triphenylamine (TPA) derivatives with mono-, di- and tri-pyridinium as substituent groups. By exchanging the negative ions ( $I^-$ ,  $BF_4^-$  and  $PF_6^-$ ) between them, a platform containing small compounds was established. After that, mammalian cells of HeLa and plant cells of BY-2 were employed for the study on cell imaging. The results clearly demonstrated that mono-pyridinium derivatives (TPA-Py- $I^-$ , TPA-Py- $BF_4^-$  and TPA-Py- $PF_6^-$ ) are mitochondrion-targeted (for HeLa cells) and cell wall-targeted (for BY-2 cells). However, both di- and tri-pyridinium substituted derivatives (TPA-diPy- $BF_4^-$  and TPA-triPy- $BF_4^-$ ) were nucleus-targeted for both cell lines. From these important findings, we can conclude that the quantity of positive charge plays a decisive role in different cell organelle-targeted staining. We also declared that our research results were very useful for designing and synthesizing probes with good cellular uptake capability, significantly enhanced targeting ability, and DNA detection.

Received 1st August 2019,  
Accepted 27th October 2019

DOI: 10.1039/c9nj03993g

rsc.li/njc

### 1. Introduction

Fluorescence cell imaging has emerged as a powerful method to provide a clear understanding of the localization,<sup>1,2</sup> concentration,<sup>3</sup> and functions<sup>4,5</sup> of biomolecules and the chemical reactions inside the cells.<sup>6</sup> In recent years, a large number of small-molecular fluorescent probes have been developed for these purposes, and their applications in the fields of biology, drug discovery,<sup>7,8</sup> and clinical diagnosis have been explored.<sup>9</sup> However, they more or less suffer from disadvantages such as difficulty to synthesize, high cost, and so on.<sup>10,11</sup> Among the current popular strategies, to achieve fluorescent materials with excellent optical performances, cationic molecules have been attracting much attention<sup>12,13</sup> due to their low cost, versatile molecular design, and interesting fluorescence property.<sup>14–16</sup> The pioneering work from Tang's group disclosed that a slight difference in the chemical structure by exchanging anions from the cationic molecules can lead to a huge difference in the optical properties of the materials.<sup>17,18</sup> Therefore, the design and synthesis of anion- $\pi^+$  interactions mediated molecules is still much required.<sup>19</sup> Furthermore, from our and other research works, we were aware that the fluorescent probes

with different quantity of positive charges play a decisive role in the specific cell organelle-targeted staining.<sup>20–22</sup> However, these studies on the primary relationships between the chemical structure and specific cell organelle-targeted staining are still limited.<sup>23,24</sup> Very desirably, if this relationship could be established, it will definitely be very useful to design and synthesize probes with improved cellular uptake capability and significantly enhanced cell target ability. Also, this relationship can benefit the study on the membrane activity and cellular functions as well.<sup>25</sup> From this point of view, we designed and synthesized a series of triphenylamine (TPA) derivatives with mono-, di- and tri-pyridinium groups, which carry one, two, and three positive charges accordingly. Moreover, by exchanging the negative ions ( $I^-$ ,  $BF_4^-$  and  $PF_6^-$ ), a small compound library with different optical behaviours was constructed. In order to evaluate the cell images of these TPA derivatives, mammalian cells (HeLa cells) and plant cells (BY-2 cells) were employed. The results demonstrated that the TPA pyridinium derivatives were readily able to penetrate into cells, and then accumulate in specific cell organelles due to the different quantity of positive charges. Clearly, due to their easy preparation, low cost, and high fluorescence quantum yields, both types of cells were very competitive with the commercially available cell staining dyes. Additionally, for the plant cell (BY-2) imaging, in accordance with the sequence of the increasing number of positive charges, fluorescence translocation from the cell wall to the nucleus was detected. This interesting result also indicated that the molecules with more positively charged pyridinium moieties

<sup>a</sup> Key Laboratory of Eco-Environment-Related Polymer Materials Ministry of Education, College of Chemistry and Chemical Engineering, Northwest Normal University, Lanzhou, 730070, China. E-mail: mahczju@hotmail.com

<sup>b</sup> Baoji AIE Research Center, College of Chemistry and Chemical Engineering, Baoji University of Arts and Sciences, Baoji, 721013, China. E-mail: qichunxuan@163.com

† Electronic supplementary information (ESI) available. See DOI: 10.1039/c9nj03993g

could dock on the surfaces and in the cavities of the negatively charged DNA *via* electrostatic interactions.

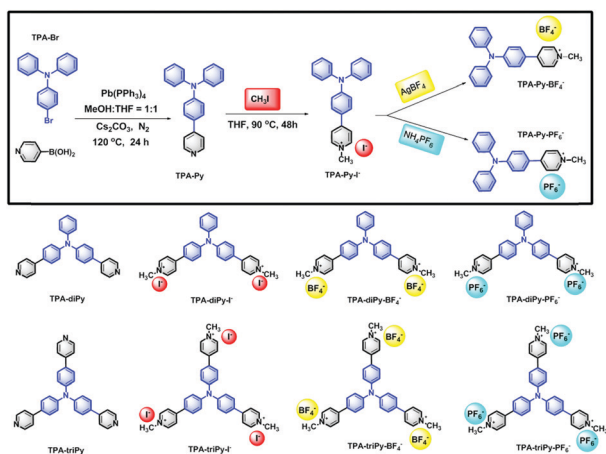
## 2. Results and discussion

### 2.1 Synthesis of all TPA derivatives

According to our previous findings, we observed that the less emissive TPA cores are highly electron rich, which could be employed as the electron-donating groups.<sup>26,27</sup> Upon connecting with the electron deficient segments, such as pyridines, the desirable fluorescence materials can be realized due to the electron donating and accepting (D–A) system formation.<sup>28,29</sup> Thereof, we synthesized the pyridine substituted TPA compound, which was termed as TPA-Py. Then, in order to elevate the electron withdrawing capability further, Menshutkin reactions between TPA-Py with  $\text{CH}_3\text{I}$  were performed, and the TPA pyridinium compound named as TPA-Py- $\text{I}^-$  was obtained. What should be noted is that the negative partners with different sizes can exert great influence on the fluorescence performance of the emitting material.<sup>17</sup> Therefore,  $\text{BF}_4^-$  and  $\text{PF}_6^-$  were selected to exchange  $\text{I}^-$ . Eventually, the ion exchanges by  $\text{AgBF}_4$  and  $\text{NH}_4\text{PF}_6$  were carried out, transforming TPA-Py- $\text{I}^-$  into TPA-Py- $\text{BF}_4^-$  and TPA-Py- $\text{PF}_6^-$ , respectively. Meanwhile, for the establishment of the primary relationship between the chemical structures with the corresponding optical behaviours, we successfully synthesized the di- and tri-pyridine modified TPA compounds, TPA-diPy and TPA-triPy, respectively. Afterwards, using both molecules as the starting materials, different negative partners ( $\text{I}^-$ ,  $\text{BF}_4^-$  and  $\text{PF}_6^-$ ) interacted pyridinium compounds were synthesized. The chemical structures are illustrated in Scheme 1. The synthetic processes plus all of the compounds' NMR and IR data are detailed in the ESI.†

### 2.2 The fluorescence performances of all TPA-derivatives in solid state and in organic solvents

With all the TPA-derivatives in hand, we first evaluated their fluorescence performances in the solid state. The corresponding maximum absorption ( $\lambda_{\text{abs}}$ ) and emission ( $\lambda_{\text{em}}$ ) wavelength,



Scheme 1 The synthesis and chemical structures of TPA derivatives.

Compounds	$\lambda_{\text{Abs}} / \text{nm}$	$\lambda_{\text{Em}} / \text{nm}$	$\Phi_{\text{F}} / \%$	Pic
TPA-Py	347	423	18.0	
TPA-Py- $\text{I}^-$	422	519	1.6	
TPA-Py- $\text{BF}_4^-$	422	536	14.2	
TPA-Py- $\text{PF}_6^-$	422	520	48.3	
-----				
TPA-diPy	362	465	28.2	
TPA-diPy- $\text{I}^-$	437	580	0.5	
TPA-diPy- $\text{BF}_4^-$	437	583	2.4	
TPA-diPy- $\text{PF}_6^-$	437	564	4.1	
-----				
TPA-triPy	359	467	1.3	
TPA-triPy- $\text{I}^-$	430	562	0.4	
TPA-triPy- $\text{BF}_4^-$	430	570	1.3	
TPA-triPy- $\text{PF}_6^-$	430	576	8.8	

Fig. 1 All TPA derivatives with the solid images under UV illumination (365 nm) and the corresponding optical properties.

as well as fluorescence quantum yields ( $\Phi$ ) are depicted in Fig. 1. In general, for the mono-substituted TPA compounds, after converting into TPA pyridinium compounds from TPA-Py, the emission wavelength red-shifted almost 100 nm. Notably, TPA-Py- $\text{BF}_4^-$  exhibited yellow emission color and had the longest emission wavelength of 536 nm. TPA-Py- $\text{PF}_6^-$  not only demonstrated a large emission wavelength of 520 nm, but also a very high fluorescence quantum yield ( $\Phi$ ) of 48.3%. From our research point, the chemical transformation that occurs with slight changes, especially in the ion exchange, is of great potential to be used to design exceptional fluorescence materials. Afterward, we extensively measured all the other compounds' fluorescence property in the solid state and found that the negative partner of  $\text{BF}_4^-$  benefited much to enhance the emission wavelength into longer range than  $\text{I}^-$  and  $\text{PF}_6^-$ . For instance, in the cases of TPA-diPy- $\text{BF}_4^-$  and TPA-triPy- $\text{BF}_4^-$ , the maximum emission wavelength could be red-shifted into 583 and 570 nm, respectively. These slight changes were very effective to generate long wavelength emitting materials, which efficiently avoided the tedious synthetic procedures. Finally, we optimized two series of compounds as the desired fluorescence materials for the ongoing research steps. The first series of compounds include TPA-Py- $\text{BF}_4^-$ , TPA-diPy- $\text{BF}_4^-$  and TPA-triPy- $\text{BF}_4^-$ . From here, we could make a clear understanding of the effect of the substituent group numbers on the bio-related applications. The other compounds included TPA-Py- $\text{I}^-$ , TPA-Py- $\text{BF}_4^-$  and TPA-Py- $\text{PF}_6^-$ . Obviously, different negative partners will possibly generate totally different applications. Then, we selected TPA-diPy- $\text{BF}_4^-$  as the representative sample to evaluate the fluorescence behavior in different solvents (Conc.: 20  $\mu\text{M}$ ,  $\lambda_{\text{ex}} = 437 \text{ nm}$ ). It can be seen from Fig. 2 that TPA-diPy- $\text{BF}_4^-$  displays the obvious solvent-dependent effect, especially in the more polar solvents, such as DMF and DMSO,

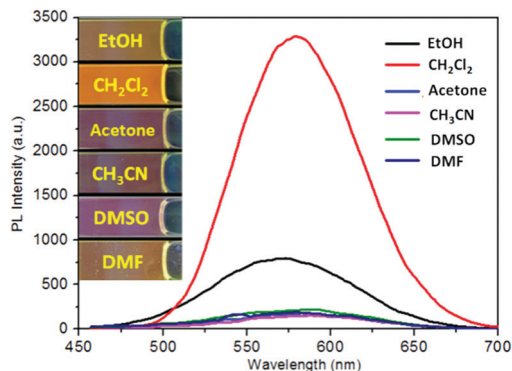


Fig. 2 The fluorescence spectrum of TPA-diPy-BF<sub>4</sub><sup>-</sup> in different solvents. (Conc.: 20 μM, λ<sub>ex</sub> = 437 nm).

where the emission was quenched largely. However, in the moderately polar solvent of CH<sub>2</sub>Cl<sub>2</sub>, TPA-diPy-BF<sub>4</sub><sup>-</sup> acted with very strong emissions. This property was probably due to the electron donor–acceptor (D–A) system formation within the molecules' structure.

### 2.3 The density functional theory (DFT) calculations of all TPA-derivatives

Meanwhile, these compounds were optimized by the density functional theory (DFT) calculations, which were carried out using the B3LYP modification with the 6-31G\* basis set in Gaussian 09. The calculated energy levels of the highest occupied molecular orbital (HOMO) and the lowest unoccupied molecular orbital (LUMO) are illustrated in Fig. 3 and Fig. S10 (ESI<sup>†</sup>). As we know, the electron withdrawing substituent is able to lower the HOMO and LUMO levels, which is due to the formation of an electron donating and accepting (D–A) system. Therefore, TPA-Py-I<sup>-</sup>, TPA-Py-BF<sub>4</sub><sup>-</sup> and TPA-Py-PF<sub>6</sub><sup>-</sup> possessed the lowest orbital energy. Accordingly, three of them had the longest emission wavelength (519 nm, 536 nm, and 520 nm, respectively). Also, after converting into TPA pyridinium compounds, the electron density was separated greatly, which indicated that TPA-Py-I<sup>-</sup>,

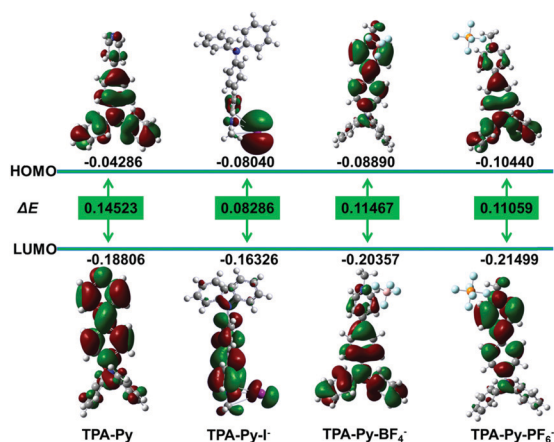


Fig. 3 HOMO–LUMO energy levels of TPA-Py, TPA-Py-I<sup>-</sup>, TPA-Py-BF<sub>4</sub><sup>-</sup> and TPA-Py-PF<sub>6</sub><sup>-</sup>, as estimated in Gaussian 09 using the B3LYP modification with the 6-31G\* basis set.

TPA-Py-BF<sub>4</sub><sup>-</sup> and TPA-Py-PF<sub>6</sub><sup>-</sup> have obvious intramolecular charge transfer (ICT) tendency.<sup>30</sup> This result was also consistent with the observed strong solvent-dependent fluorescence behaviors.

### 2.4 The toxicity evaluation and the mammalian cell staining by TPA derivatives

It was of high importance that the fluorescent materials have better biocompatibility with low toxicity to target bio substrates.<sup>31–33</sup> The metabolic viability of the HeLa cells and after incubating with TPA derivatives was determined through methylthiazolyldiphenyl-tetrazolium bromide (MTT) assays to evaluate the cytotoxicity of these compounds.<sup>34</sup> The results demonstrated that the cell viability remains above 85% after a 96 h incubation with TPA-Py-I<sup>-</sup>, TPA-Py-BF<sub>4</sub><sup>-</sup>, TPA-Py-PF<sub>6</sub><sup>-</sup>, TPA-diPy-BF<sub>4</sub><sup>-</sup> and TPA-triPy-BF<sub>4</sub><sup>-</sup>, respectively, at different concentrations (Fig. S15, ESI<sup>†</sup>), indicating that these TPA derivatives are of low cytotoxicity within the testing window. In the ongoing cell staining experiment, we decided the working concentration of all TPA compounds as 10 μM. Fig. 4 displays the fluorescence image of the HeLa cells incubated with probes for 30 min at a temperature of 37 °C. Obviously, the bright fluorescence images were observed inside the cells, indicating that all the probes successfully penetrated the cell membrane and accumulate in specific cell organelles under physiological conditions. According to our and other groups' research results, we postulated that these different cell organelle-targeted staining might come from the positive charges of the pyridinium moieties and the target-specific interactions between probes and biomolecules.<sup>20,23</sup> Especially, in the cases of TPA-Py-I<sup>-</sup>, TPA-Py-BF<sub>4</sub><sup>-</sup>, and TPA-Py-PF<sub>6</sub><sup>-</sup>, the reticulum structures of mitochondria from the HeLa cells are clearly visible in the presence of the bright yellow fluorescence of TPA-Py-I<sup>-</sup>, TPA-Py-BF<sub>4</sub><sup>-</sup> and TPA-Py-PF<sub>6</sub><sup>-</sup>. Very notably, TPA-diPy-BF<sub>4</sub><sup>-</sup> and TPA-triPy-BF<sub>4</sub><sup>-</sup> carries two and three positive charges, respectively, which allow them to penetrate the cell nucleus very specifically. Due to the very large Stokes shift over 135 nm, the captured pictures are very sharp-edged and with ignored background noise. Therefore, those small molecules with different quantity of positive charges are well-suited imaging agents for mitochondrial and cell nucleus targeting, and also for the cell morphological change

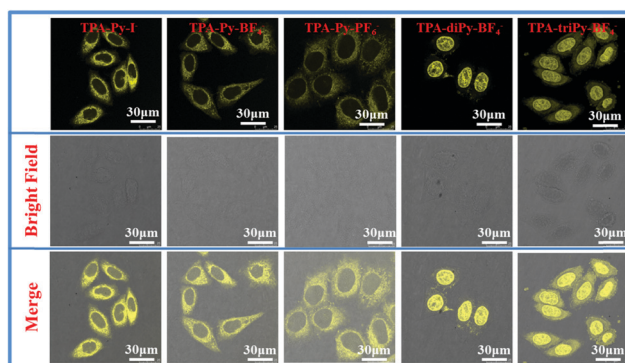


Fig. 4 Fluorescence images of HeLa cells stained with 10 μM TPA-Py-I<sup>-</sup>, TPA-Py-BF<sub>4</sub><sup>-</sup>, TPA-Py-PF<sub>6</sub><sup>-</sup>, TPA-diPy-BF<sub>4</sub><sup>-</sup>, TPA-triPy-BF<sub>4</sub><sup>-</sup> for 30 min respectively.

tracking. From this result, we were able to establish the primary relationship between the chemical structures and the specific cell organelle-targeted staining. This important finding is very useful to design and synthesize probes with improved cellular uptake capability and significantly enhanced target ability.

## 2.5 The co-staining of TPA-Py-I<sup>-</sup> and TPA-Py-BF<sub>4</sub><sup>-</sup> with mitochondria and nucleus-specific dyes

To confirm the specific staining of mitochondria by probes of TPA-Py-I<sup>-</sup> and TPA-Py-BF<sub>4</sub><sup>-</sup> respectively, the Mito Tracker Red, a commercially available dye for mitochondria staining was used; Hoechst 33342, a commercially available dye for nucleus staining was co-used as a calibration to stain the HeLa cells. From the staining images (Fig. 5 and 6), we can see that TPA-Py-I<sup>-</sup> and TPA-Py-BF<sub>4</sub><sup>-</sup> have penetrated smoothly into the mitochondria very specifically. The green (FL from probes received at 510–540 nm) and red fluorescence (FL from Mito Tracker Red received at 590–610 nm) could be recorded in the mitochondria

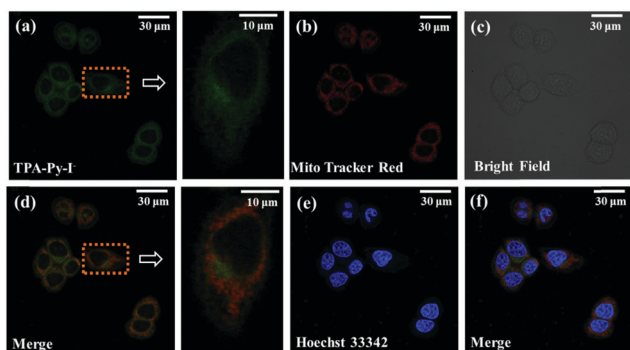


Fig. 5 CLSM images of HeLa cells. (a) Stain with 10  $\mu\text{M}$  TPA-Py-I<sup>-</sup> for 30 min, nearby is a partial enlarged picture; (b) co-staining with 50 nM mitochondrion-specific dye Mito Tracker Red; (c) bright field; (d) the overlay images of a and b; (e) co-staining with 5  $\mu\text{g ml}^{-1}$  nucleus-specific dye Hoechst 33342; (f) The overlay images of a, b, e. (Excitation wavelength: 405 nm; emission filter: 460–560 nm; irradiation time: 15.49 s per scan.)

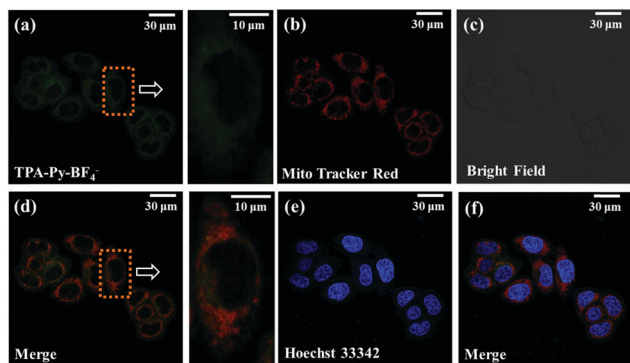


Fig. 6 CLSM images of HeLa cells. (a) Stain with 10  $\mu\text{M}$  TPA-Py-BF<sub>4</sub><sup>-</sup> for 30 min, nearby is a partial enlarged picture; (b) co-staining with 50 nM mitochondrion-specific dye Mito Tracker Red; (c) bright field; (d) the overlay images of a and b; (e) co-staining with 5  $\mu\text{g ml}^{-1}$  nucleus-specific dye Hoechst 33342; (f) the overlay images of a, b, e. (Excitation wavelength: 405 nm; emission filter: 460–560 nm; irradiation time: 15.49 s per scan.)

by an excellent overlap. Thus, our probes of TPA-Py-I<sup>-</sup> and TPA-Py-BF<sub>4</sub><sup>-</sup> could be employed as mitochondria staining dyes, which are almost competitive with the commercially available Mito Tracker Red due to an easier synthetic process, and also the lower cost. It was well known that their mitochondria-targeting behaviour could be attributed to the electrostatic interaction between the negative transmembrane potential of the mitochondria within a cancer cell and positively charged pyridinium moiety. However, we found that only the well-matched interactions are able to accelerate the mitochondria-targeted imaging because TPA-diPy-BF<sub>4</sub><sup>-</sup> and TPA-triPy-BF<sub>4</sub><sup>-</sup> acted as cell nucleus-targeted staining agents, which is due to their more positive charges.

## 2.6 The co-staining of TPA-diPy-BF<sub>4</sub><sup>-</sup>, and TPA-triPy-BF<sub>4</sub><sup>-</sup> with nucleus-specific dyes

Up to now, we have disclosed an important generality that the mono-pyridinium substituted TPA compounds could be employed as mitochondria staining dyes.<sup>35,36</sup> However, for TPA-diPy-BF<sub>4</sub><sup>-</sup> and TPA-triPy-BF<sub>4</sub><sup>-</sup>, both of them carries two and three positive charges, respectively, which allowed them to penetrate the cell nucleus very specifically as seen in cell imaging (Fig. 4). Through the co-staining experiments (Fig. 7), it can be seen that TPA-diPy-BF<sub>4</sub><sup>-</sup> and TPA-triPy-BF<sub>4</sub><sup>-</sup> selectively accumulate in the nucleus with extraordinary emission color, which taken a very sharp contrast with the commercially available dye of Hoechst 33342 with a very dark blue emission color. Moreover, the longer absorption wavelength of our probes was more beneficial to protect the cells from further photobleaching than Hoechst 33342 (350 nm). Once again, thereof, we established the primary relationship between the chemical structures and the cell organelle-targeted staining.

The cell staining experiments verified that the multiple cation-charged molecules were very cell-membrane permeable. Also, the positively charged molecules could specifically accumulate on the cell nucleus. It was found that the DNA, one of the most abundant components in the nucleus, exhibited a high affinity for the cationic molecules *via* the electrostatic force.<sup>37</sup> Therefore, the molecules with more positively charged pyridinium moieties could dock on the surfaces and in the cavities of the negatively charged DNA *via* electrostatic interactions, leading to the cell

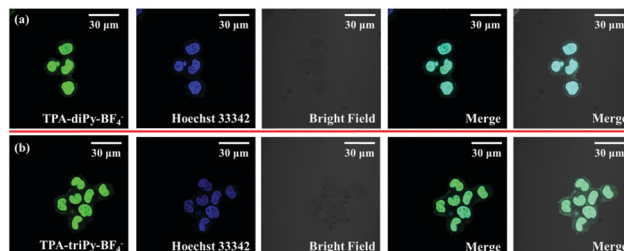


Fig. 7 CLSM images of HeLa cells. (a) Co-staining of Hoechst 33342 (5  $\mu\text{g ml}^{-1}$ ) with TPA-diPy-BF<sub>4</sub><sup>-</sup> (10  $\mu\text{M}$ ) and the overlay images; (b) co-staining of Hoechst 33342 (5  $\mu\text{g ml}^{-1}$ ) with TPA-triPy-BF<sub>4</sub><sup>-</sup> (10  $\mu\text{M}$ ) and the overlay images. (Excitation wavelength: 454 nm; emission filter: 480–580 nm; irradiation time: 15.49 s per scan.)

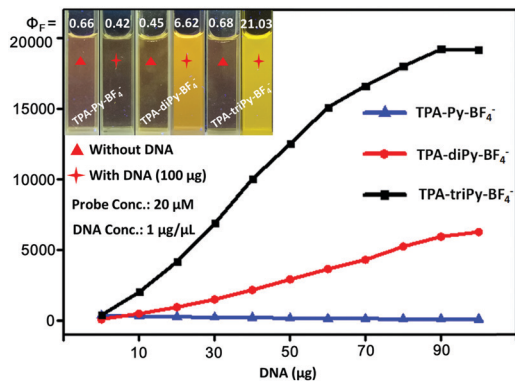


Fig. 8 PL spectra of TPA-py-BF<sub>4</sub><sup>-</sup>, TPA-diPy-BF<sub>4</sub><sup>-</sup>, TPA-triPy-BF<sub>4</sub><sup>-</sup> upon the addition of DNA in dilute solvents.

nucleus-targeted staining with enhanced emission intensity (Fig. 8). As a result, the cationic fluorescence materials (TPA-diPy-BF<sub>4</sub><sup>-</sup> and TPA-triPy-BF<sub>4</sub><sup>-</sup>) can be applied as probes to detect the negatively charged biomacromolecules, such as DNA.

### 2.7 Plant cell staining by TPA derivatives

Fluorescence staining has been widely used to observe plant cell development, apoptosis and protein interactions.<sup>38,39</sup> For example, fluorescein diacetate, propidium iodide (PI), DCFH-DA as well as FM4-64 were used previously.<sup>40,41</sup> However, some problems still existed in practical applications. For example, upon staining, the boundaries of the subcellular structures in the cells were blurred and could not be clearly distinguished. Also, the establishment of a primary relationship between the chemical structures with the subcellular-targeted staining was much required. Therefore, we employed TPA-Py-I<sup>-</sup>, TPA-Py-BF<sub>4</sub><sup>-</sup>, TPA-Py-PF<sub>6</sub><sup>-</sup>, TPA-diPy-BF<sub>4</sub><sup>-</sup> and TPA-triPy-BF<sub>4</sub><sup>-</sup> to stain with Tobacco cells (*Nicotiana tabacum* L. cv. Bright Yellow 2 [BY-2]) for 30 min; then, the suspending liquids were washed by PBS buffer solution several times. The images of the treated cells were taken to immediate imaging by a digital camera (ECLIPSE Ts2-FL, Nikon-FL) under UV light. We can see from Fig. 9 that in the cases of TPA-Py-I<sup>-</sup>, TPA-Py-BF<sub>4</sub><sup>-</sup> and TPA-Py-PF<sub>6</sub><sup>-</sup>, the cell walls were clearly exhibited, which was due to the adsorption of the fluorescence materials on the surface of the cells. Probably the electrostatic attraction, the van der Waals force, and H-bonding play an important role during the staining process. In sharp contrast, in the case of TPA-triPy-BF<sub>4</sub><sup>-</sup>, the cellular uptake and distribution profile was very different. The TPA-triPy-BF<sub>4</sub><sup>-</sup> could penetrate the cells, and then accumulate in the nucleus very specifically. Although the co-staining experiment with the blue

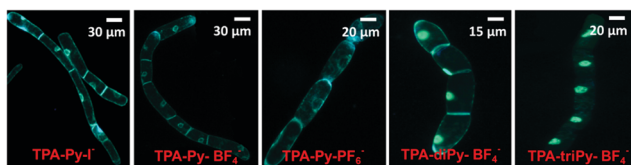


Fig. 9 Fluorescence images of BY-2 cells treated with dyes at room temperature for 10 min.

emission of DAPI has not been applied, TPA-triPy-BF<sub>4</sub><sup>-</sup> was a cell nucleus targeted probe with a high visualization ability and retention ability with minimum background staining. Compared to the highly toxic and expensive commercially available DAPI, TPA-triPy-BF<sub>4</sub><sup>-</sup> was confirmed as a promising alternative for nucleus-specific plant cell imaging. In summary, we can conclude from these research results that the chemical structures, especially the electron charges, play a decisive role for the different subcellular-targeted staining. Possibly, the multiple cationic TPA-triPy-BF<sub>4</sub><sup>-</sup> was of a close affinity with the DNA in the living cells, which led to the nucleus-specific plant cell imaging.

## 3. Conclusions

In summary, we synthesized a series of TPA derivatives with mono-, di- and tri-pyridinium as substituent groups. By exchanging the negative ions (I<sup>-</sup>, BF<sub>4</sub><sup>-</sup> and PF<sub>6</sub><sup>-</sup>) between them, a series of TPA compounds with different optical behaviors was obtained. These results demonstrated that a slight structural difference is of great influence on the materials from the aspect of emission wavelength and intensity. For the purpose of evaluating their potential biological applications, we employed TPA pyridinium derivatives with different cationic charges in cell staining. The cells included the mammalian cells of HeLa and plant cells of BY-2. As a generality, TPA-Py-I<sup>-</sup>, TPA-Py-BF<sub>4</sub><sup>-</sup> and TPA-Py-PF<sub>6</sub><sup>-</sup> were mitochondrion-targeted (for HeLa cells) and cell wall-targeted (for BY-2 cells) respectively, while both TPA-diPy-BF<sub>4</sub><sup>-</sup> and TPA-triPy-BF<sub>4</sub><sup>-</sup> were nucleus-targeted in the case of fixed HeLa cells and BY-2 cells. From these research results, we were able to establish two important research findings: (1) the primary relationship between the chemical structures and the specific organelle-targeted staining for mammalian cells and plant cells; (2) the positive charges play an important role in DNA detection in cells and *in vitro*. Therefore, our important findings were very useful to design and synthesize probes with improved cellular uptake capability, and significantly enhanced cell target ability, which definitely benefited the study on the membrane activity, cellular functions, and DNA detection.

## 4. Materials and methods

### 4.1 Materials

4-Bromo-*N,N*-diphenylaniline (98%), tris(4-bromophenyl)amine (98%), bis(4-bromophenyl)amine, pyridine-4-boronic acid (99%), iodobenzene (99%), cesium carbonate (Cs<sub>2</sub>CO<sub>3</sub>, 99%), tetrakis(triphenylphosphine)palladium(0) (Pb(PPh<sub>3</sub>)<sub>4</sub>, 98%), potassium hydroxide (KOH), iodomethane (99.5%), 1,10-phenanthroline monohydrate, cuprous iodide (CuI, 99%), silver tetrafluoroborate (AgBF<sub>4</sub>, 99%), and ammonium hexafluorophosphate (NH<sub>4</sub>PF<sub>6</sub>, 99%), were purchased from Aladdin Co. Nitrogen with a purity of 99.99% was provided from a commercial source. Other reagents, such as methanol, tetrahydrofuran (THF), dichloromethane (DCM), acetonitrile, toluene, ethanol, dichloromethane, and dimethyl sulfoxide (DMSO) were of analytical grade and were purchased from Energy Chemical Company.

## 4.2 Instrumentation

$^1\text{H}$  NMR (600 MHz) and  $^{13}\text{C}$  NMR (150 MHz) spectra were recorded on a mercury spectrometer at 25 °C, and all NMR spectra were referenced to the solvent. UV-Visible absorption spectra (UV) were recorded on a TU-1901 spectrometer. Fluorescence spectra and fluorescence quantum yields were measured using a FluoroSENS 9003 Fluorescence Spectrophotometer. Fluorescence microscopy images of the HeLa cells were taken on DM5000B (Leica, Germany). Co-staining fluorescence microscopy images of HeLa cells were taken on IX71 (Leica, Germany). All the samples were prepared according to the standard methods.

## 4.3 Cytotoxicity

The cytotoxicity test was performed with the HeLa cells. TPA-Py-I<sup>-</sup>, TPA-Py-BF<sub>4</sub><sup>-</sup>, TPA-Py-PF<sub>6</sub><sup>-</sup>, TPA-diPy-BF<sub>4</sub><sup>-</sup> and TPA-triPy-BF<sub>4</sub><sup>-</sup> were sterilized with ultraviolet light and dissolved in DMSO. Then, the solution was diluted with PBS buffer (pH = 7.4) to different concentrations (0, 10, 20, 30, 40 and 50 μmol mL<sup>-1</sup>). To obtain complete cell culture medium, 10% FBS, 100 units mL<sup>-1</sup> penicillin, and 100 units mL<sup>-1</sup> streptomycin were added in the mixture. The HeLa cells were cultured in the conditioned medium at 37 °C in a humidified environment of 95% O<sub>2</sub> and 5% CO<sub>2</sub>. After 24 h of incubation, the cell viability was determined by the 3-(4,5-dimethylthiazol-2-yl)-2,5-diphenyltetrazolium bromide (MTT) method.

## 4.4 Cell fluorescence imaging

Take a bottle of HeLa cells in the log phase, remove the old medium, wash the cells once with 3 mL of PBS, add 1 mL of 0.25% trypsin, let stand for 3 min, and remove the trypsin. Add 1 mL of DMEM medium and mix well. Add 30 μL of HeLa cells and 1 mL of basic medium to each culture dish. 37 °C 5% CO<sub>2</sub> overnight. Add 980 μL of medium to 20 μL of TPA-Py-I<sup>-</sup>, TPA-Py-BF<sub>4</sub><sup>-</sup>, TPA-Py-PF<sub>6</sub><sup>-</sup>, TPA-diPy-BF<sub>4</sub><sup>-</sup> and TPA-triPy-BF<sub>4</sub><sup>-</sup> (10 μM) for 30 minutes at 37 °C 5% CO<sub>2</sub>, remove the old medium and wash 2–3 times with PBS, fix with 4% paraformaldehyde for 20 minutes, wash with PBS 2–3 times, test on the machine.

## 4.5 Cell counterstain with Hoechst 33342 and Mito Tracker Red

Cells were first stained in the desired concentration by following the previous staining procedure. Cells were then incubated at 37 °C in 5% CO<sub>2</sub> for 30 min and imaged at ambient temperature in the medium. The imaging of Hoechst 33342 counterstain followed a similar procedure. The final concentration of Hoechst 33342 was 1 μg mL<sup>-1</sup>. Before imaging, the cells were rinsed by PBS twice after 10 minutes. The use of the Mito Tracker Red (10 μg mL<sup>-1</sup>) is the same as the usage of the Hoechst 33342.

## 4.6 *Nicotiana tabacum* L. cv. Bright Yellow-2

The suspension cells were placed in MS liquid medium (pH 5.8) supplemented with 3% (w/v) sucrose and 0.4 mg L<sup>-1</sup>, 2,4-dichlorophenoxyacetic acid (2,4-D) (Sigma- In Aldrich). The shake culture was carried out in the dark at 25 °C (oscillation rate 130 rpm). 10 mL of cell culture was pipetted every 7 days and transferred

to 1000 mL of fresh MS medium for subculture. All the operations were done under aseptic conditions.

## 4.7 Suspension cell treatment

Take a volume of cell suspension in the log phase of growth, dilute and shake well with deionized water in a volume ratio of 1 : 3 before use; 50 μL of TPA-Py-I<sup>-</sup>, TPA-Py-BF<sub>4</sub><sup>-</sup>, TPA-Py-PF<sub>6</sub><sup>-</sup>, TPA-diPy-BF<sub>4</sub><sup>-</sup>, TPA-triPy-BF<sub>4</sub><sup>-</sup> and TPA derivatives/F-127 nanomicelles was added to 1 mL of suspension cells. Incubate for 0.5 h at 25 °C in the dark; filter and wash 1 to 3 times with deionized water. Suspension cell fluid was treated with an equal volume of deionized water as a control.

## 4.8 Synthesis of TPA-Py, TPA-diPy, and TPA-triPy<sup>42</sup>

Into a 250 mL three-necked round-bottom flask, 4-bromo-*N,N*-diphenylaniline (6 mmol, 331.2 g mol<sup>-1</sup>, 1.987 g), pyridine-4-boronic acid (8 mmol, 122.9 g mol<sup>-1</sup>, 0.983 g), cesium carbonate (6 mmol, 325.8 g mol<sup>-1</sup>, 1.955 g) and tetrakis(triphenylphosphine)-palladium(0) (0.3 mmol, 1155 g mol<sup>-1</sup>, 5% equiv., 0.347 g) was added. Then the mixture of THF (75 mL) and MeOH (75 mL) were added. The mixture was refluxed at 120 °C for 36 h under N<sub>2</sub> atmosphere. The reaction mixture was concentrated by rotary evaporation. *N,N*-diphenyl-4-(pyridin-4-yl)aniline was purified by column chromatography on silica gel (200–300 mesh) with a mixture of petroleum ether and ethyl acetate as the eluent (20 : 1 by volume), obtaining a white solid (1.5 g, 77% yield).  $^1\text{H}$  NMR (600 MHz, CDCl<sub>3</sub>) δ (TMS, ppm): 8.60 (d, *J* = 6.0 Hz, 2H), 7.51 (d, *J* = 8.5 Hz, 2H), 7.46 (d, *J* = 6.0 Hz, 2H), 7.29 (t, *J* = 7.7 Hz, 4H), 7.13 (dd, *J* = 8.0, 4.2 Hz, 6H), 7.07 (t, *J* = 7.3 Hz, 2H).

The synthetic process of TPA-diPy and TPA-triPy is the same as the above mentioned method. TPA-diPy was a yellow solid (0.68 g, 77% yield).  $^1\text{H}$  NMR (600 MHz, CDCl<sub>3</sub>) δ (TMS, ppm): 8.63 (d, *J* = 6.0 Hz, 4H), 7.56 (d, *J* = 8.6 Hz, 4H), 7.48 (d, *J* = 6.0 Hz, 4H), 7.33 (t, *J* = 7.8 Hz, 2H), 7.22–7.17 (m, 6H), 7.14 (t, *J* = 7.4 Hz, 1H). TPA-triPy was a yellow solid (1.19 g, 60% yield).  $^1\text{H}$  NMR (600 MHz, CDCl<sub>3</sub>) δ (TMS, ppm): 8.65 (d, *J* = 6.2 Hz, 6H), 7.60 (d, *J* = 11.4 Hz, 6H), 7.50 (d, *J* = 6.2 Hz, 6H), 7.27 (d, *J* = 8.7 Hz, 6H).

## 4.9 Synthesis of TPA-Py-I<sup>-</sup>, TPA-diPy-I<sup>-</sup>, and TPA-triPy-I<sup>-43</sup>

Into a 100 mL round-bottom flask, TPA-Py (3 mmol, 322.4 g mol<sup>-1</sup>, 0.967 g), iodomethane (4.5 mmol, 141.9 g mol<sup>-1</sup>, 0.639 g) and THF (50 mL) was added. Then, the mixture was stirred at 90 °C for 36 h. After that, the reaction mixture was precipitated from THF (dry), and washed using THF and *n*-hexane several times. A yellow solid powder was obtained by filtration and dried under vacuum at 30 °C overnight. TPA-Py-I<sup>-</sup> was a yellow solid (1.183 g, 85% yield).  $^1\text{H}$  NMR (600 MHz, CDCl<sub>3</sub>) δ (TMS, ppm): 8.99 (d, *J* = 7.0 Hz, 2H), 8.04 (d, *J* = 7.1 Hz, 2H), 7.66–7.63 (m, 2H), 7.39–7.31 (m, 4H), 7.22–7.13 (m, 6H), 7.09–7.05 (m, 2H), 4.55 (s, 3H).

The synthetic process of TPA-diPy-I<sup>-</sup> and TPA-triPy-I<sup>-</sup> is the same as the above mentioned method. TPA-diPy-I<sup>-</sup> was an orange solid (0.27 g, 79% yield).  $^1\text{H}$  NMR (600 MHz, D<sub>2</sub>O) δ (TMS, ppm): 8.67 (d, *J* = 6.9 Hz, 4H), 8.24 (d, *J* = 7.1 Hz, 4H), 7.94 (d, *J* = 8.9 Hz, 4H), 7.53–7.49 (m, 2H), 7.37 (dd, *J* = 13.2, 8.2 Hz, 6H), 7.34 (s, 1H), 4.33 (s, 6H). TPA-triPy-I<sup>-</sup> was a red solid (0.45 g, 80% yield).

$^1\text{H}$  NMR (600 MHz, DMSO- $d_6$ )  $\delta$  (TMS, ppm): 8.95 (d,  $J$  = 6.9 Hz, 6H), 8.45 (d,  $J$  = 7.0 Hz, 6H), 8.12 (d,  $J$  = 8.8 Hz, 6H), 7.34 (d,  $J$  = 8.8 Hz, 6H), 4.29 (s, 9H).

#### 4.10 Synthesis of TPA-Py-BF $_4^-$ , TPA-diPy-BF $_4^-$ , and TPA-triPy-BF $_4^-$

Into a 100 mL round-bottom flask, TPA-Py-I $^-$  (0.7 mmol, 464.3 g mol $^{-1}$ , 0.325 g) and dichloroethane (30 mL) was added. Further, AgBF $_4$  (1.4 mmol, 194.7 g mol $^{-1}$ , 0.273 g) was taken in a vial and dichloroethane (2 mL) was added. Then, the AgBF $_4$  solution was added dropwise to the round-bottom flask using a syringe. The reaction was stirred at room temperature for 48 hours. Then, the mixture was extracted by adding water. The organic phase was separated and concentrated by rotary evaporation. The solid was dried under vacuum at 30 °C overnight. TPA-Py-BF $_4^-$  was a yellow solid (0.232 g, 78% yield).  $^1\text{H}$  NMR (600 MHz, CDCl $_3$ )  $\delta$  (TMS, ppm): 8.57 (d,  $J$  = 6.9 Hz, 2H), 7.99 (d,  $J$  = 7.0 Hz, 2H), 7.63 (d,  $J$  = 9.0 Hz, 2H), 7.37–7.33 (m, 4H), 7.23–7.15 (m, 6H), 7.07 (d,  $J$  = 8.9 Hz, 2H), 4.36 (s, 3H).

The synthetic process of TPA-diPy-BF $_4^-$  and TPA-triPy-BF $_4^-$  is the same as the above mentioned method. TPA-diPy-BF $_4^-$  was a brown solid (0.23 g, 76% yield).  $^1\text{H}$  NMR (600 MHz, D $_2$ O)  $\delta$  (TMS, ppm): 8.67 (d,  $J$  = 6.9 Hz, 4H), 8.24 (d,  $J$  = 7.0 Hz, 4H), 7.94 (d,  $J$  = 8.9 Hz, 4H), 7.52–7.48 (m, 2H), 7.41–7.28 (m, 7H), 4.33 (s, 6H). TPA-triPy-BF $_4^-$  was a brown solid (0.37 g, 75% yield).  $^1\text{H}$  NMR (600 MHz, DMSO- $d_6$ )  $\delta$  (TMS, ppm): 8.94 (d,  $J$  = 6.8 Hz, 6H), 8.44 (d,  $J$  = 6.8 Hz, 6H), 8.12 (d,  $J$  = 8.7 Hz, 6H), 7.34 (d,  $J$  = 8.7 Hz, 6H), 4.29 (s, 9H).

#### 4.11 Synthesis of TPA-Py-PF $_6^-$ , TPA-diPy-PF $_6^-$ , and TPA-triPy-PF $_6^-$

Into a 100 mL round-bottom flask, TPA-Py-I $^-$  (0.7 mmol, 464.3 g mol $^{-1}$ , 0.325 g) and acetonitrile (30 mL) was added. Further, NH $_4$ PF $_6^-$  (1.75 mmol, 163 g mol $^{-1}$ , 0.285 g) was taken in a vial and deionized water (10 mL) was added. Then, the NH $_4$ PF $_6^-$  solution was added dropwise to the round-bottom flask using a syringe. The reaction was stirred at room temperature for 48 hours. After the reaction, the mixture was extracted by adding water. The organic phase was separated and concentrated by rotary evaporation. The solid was dried under vacuum at 30 °C overnight. TPA-Py-PF $_6^-$  was a yellow solid (0.280 g, 83% yield).  $^1\text{H}$  NMR (600 MHz, CDCl $_3$ )  $\delta$  (TMS, ppm): 8.44 (d,  $J$  = 7.0 Hz, 2H), 7.98 (d,  $J$  = 7.1 Hz, 2H), 7.65–7.62 (m, 2H), 7.38–7.34 (m, 4H), 7.22–7.15 (m, 6H), 7.07 (d,  $J$  = 9.0 Hz, 2H), 4.32 (s, 3H).

The synthetic process of TPA-diPy-PF $_6^-$  and TPA-triPy-PF $_6^-$  is the same as the above mentioned method. TPA-diPy-PF $_6^-$  was an orange solid (0.27 g, 75% yield).  $^1\text{H}$  NMR (600 MHz, D $_2$ O)  $\delta$  (TMS, ppm): 8.67 (d,  $J$  = 7.0 Hz, 4H), 8.24 (d,  $J$  = 7.1 Hz, 4H), 7.94 (d,  $J$  = 8.8 Hz, 4H), 7.52–7.49 (m, 2H), 7.40–7.32 (m, 7H), 4.33 (s, 6H). TPA-triPy-PF $_6^-$  was an orange solid (0.43 g, 72% yield).  $^1\text{H}$  NMR (600 MHz, DMSO- $d_6$ )  $\delta$  (TMS, ppm): 8.94 (d,  $J$  = 6.8 Hz, 6H), 8.44 (d,  $J$  = 7.0 Hz, 6H), 8.12 (d,  $J$  = 8.8 Hz, 6H), 7.34 (d,  $J$  = 8.8 Hz, 6H), 4.29 (s, 9H).

#### 4.12 Synthesis of 4-bromo-*N*-(4-bromophenyl)-*N*-phenylaniline<sup>44</sup>

Into a 100 mL round-bottom flask, bis(4-bromophenyl) amine (3 mmol, 327 g mol $^{-1}$ , 0.981 g), iodobenzene (3.6 mmol, 204 g mol $^{-1}$ , 0.734g), 1,10-phenanthroline monohydrate

(0.6 mmol, 198 g mol $^{-1}$ , 0.119 g), cuprous iodide (0.3 mmol, 191 g mol $^{-1}$ , 0.057 g), potassium hydroxide (6 mmol, 56 g mol $^{-1}$ , 0.336 g), and toluene (20 mL) was added. Then, the mixture was refluxed at 125 °C for 4 h. The reaction mixture was concentrated by rotary evaporation. 4-Bromo-*N*-(4-bromophenyl)-*N*-phenylaniline was purified by column chromatography on silica gel (200–300 mesh) with a mixture of petroleum ether and ethyl acetate as the eluent (50 : 1 by volume); the solid was dried under vacuum at 30 °C overnight, obtaining a white solid (0.9 g, 75% yield).  $^1\text{H}$  NMR (600 MHz, DMSO- $d_6$ )  $\delta$  (TMS, ppm): 7.47–7.44 (m, 4H), 7.36–7.32 (m, 2H), 7.11 (t,  $J$  = 7.4 Hz, 1H), 7.06–7.03 (m, 2H), 6.95–6.92 (m, 4H).

## Conflicts of interest

There are no conflicts to declare.

## Acknowledgements

This work is supported by the National Natural Science Foundation of China (no. 21764012). We thank the Key Laboratory of EcoEnvironment-Related Polymer Materials (Northwest Normal University) and the Ministry of Education Scholars Innovation Team (IRT 1177) for financial support. We also thank Prof. Anjun, Qin, Dr Rong, Hu from SCUT (South China University of Technology) and Prof. Dongfeng Dang, Dr Dehuai Li from Xi'an Jiaotong University for their help and comments.

## Notes and references

- 1 J. Mei, Y. Huang and H. Tian, *ACS Appl. Mater. Interfaces*, 2018, **10**, 12217–12261.
- 2 H. Zhu, J. Fan, J. Du and X. Peng, *Acc. Chem. Res.*, 2016, **49**, 2115–2126.
- 3 H. Singh, S. Sreedharan, R. Tiwari, C. Walther, C. Smythe, S. K. Pramanik, J. Thomas and A. A. Das, *Cryst. Growth Des.*, 2018, **18**, 7199–7206.
- 4 J. Li, N. Kwon, Y. Jeong, S. Lee, G. Kim and J. Yoon, *ACS Appl. Mater. Interfaces*, 2018, **10**, 12150–12154.
- 5 N. Alifur, A. Zebibula, J. Qi, H. Zhang, C. Sun, X. Yu, D. Xue, J. Lam, G. Li, J. Qian and B. Z. Tang, *ACS Nano*, 2018, **12**, 11282–11293.
- 6 N. An, Q. Zhang, J. Wang, C. Liu, L. Shi, L. Liu, L. Deng and Y. Lu, *Polym. Chem.*, 2017, **8**, 1138–1145.
- 7 A. Sharma, J. F. Arambula, S. Koo, R. Kumar, H. Singh, J. L. Sessler and J. S. Kim, *Chem. Soc. Rev.*, 2019, **48**, 771–813.
- 8 M. R. L. Stone, M. S. Butler, W. Phetsang, M. Cooper and M. Blaskovich, *Trends Biotechnol.*, 2018, **36**, 523–536.
- 9 A. Mochida, F. Ogata, T. Nagaya, P. L. Choyke and H. Kobayash, *Bioorg. Med. Chem.*, 2018, **26**, 925–930.
- 10 W. Phetsang, R. Pelington, M. Butler, S. KC, M. Pitt, G. Kaeslin, M. A. Cooper and M. A. T. Blaskovich, *ACS Infect. Dis.*, 2016, **2**, 688–701.
- 11 C. Wang, Y. Lu, S. Cai, W. Long, Y. Zheng, J. Lin, Y. Yan, X. Huang, W. Wong, K. Zhang and C. Chow, *Sens. Actuators, B*, 2018, **262**, 386–394.

- 12 Y. Orimoto, K. Ishimoto and Y. Aoki, *J. Phys. Chem. C*, 2018, **122**, 4546–4556.
- 13 N. Inada, N. Fukuda, T. Hayashi and S. Uchiyama, *Nat. Protoc.*, 2019, **14**, 1293.
- 14 H. Ma, Z. Yang, H. Cao, L. Lei, L. Chang, Y. Ma, M. Yang, X. Yao, Q. Sun and Z. Lei, *J. Mater. Chem. B*, 2017, **5**, 655–660.
- 15 N. Zhao, S. Chen, Y. Hong and B. Z. Tang, *Chem. Commun.*, 2015, **51**, 13599–13602.
- 16 K. Vahedi, S. Sharifi, K. Alizadeh, O. Marti and M. Amirkhani, *Opt. Quantum Electron.*, 2018, **50**, 24.
- 17 X. Gong, Q. L. Zhang, S. Zhang, Y. Xia, Q. Bai, S. Chen and X. L. Ni, *Dyes Pigm.*, 2019, **163**, 502–508.
- 18 J. Xue, W. Bai, H. Duan, J. Nie, B. Du, J. Z. Sun and B. Z. Tang, *Macromolecules*, 2018, **51**, 5762–5772.
- 19 Q. Lin, G. F. Gong, Y. Q. Fan, Y. Y. Chen, J. Wang, X. W. Guan, J. Liu, Y. M. Zhang, H. Yao and T. B. Wei, *Chem. Commun.*, 2019, **55**, 3247–3250.
- 20 H. Ma, M. Yang, C. Zhang, Y. Ma, Y. Qin, Z. Lei, L. Chang, L. Lei, T. Wang and Y. Yang, *J. Mater. Chem. B*, 2017, **5**, 8525–8531.
- 21 J. Y. Hyun, N. R. Kang and I. Shin, *Org. Lett.*, 2018, **20**, 1240–1243.
- 22 C. Xu, D. Li, Z. Cao, M. Xiong, X. Yang and J. Wang, *Nano Lett.*, 2019, **19**, 2688–2693.
- 23 P. Gao, W. Pan, N. Li and B. Tang, *Chem. Sci.*, 2019, **10**, 6035–6071.
- 24 K. Singh, S. Singh, P. Srivastava, S. Sivakumar and A. K. Patra, *Chem. Commun.*, 2017, **53**, 6144–6147.
- 25 F. Hu, G. Zhang, C. Zhan, W. Zhan, Y. Yan, Y. Zhao, H. Fu and D. Zhang, *Small*, 2015, **11**, 1335–1344.
- 26 E. Catal, E. Keles, N. Seferoğlu, S. Achelle, A. Barsella, F. R. L. Guen and Z. Seferoğlu, *New J. Chem.*, 2018, **42**, 15052–15060.
- 27 H. Ma, M. Yang, S. Zhang, P. Yin, T. Wang, Y. Yang, Z. Lei, Y. Ma, Y. Qin and Z. Yang, *Analyst*, 2019, **144**, 536–542.
- 28 X. Cao, X. Zhang, M. Wang, D. Shi, Q. Wu, Y. Tao and W. Huang, *Org. Electron.*, 2018, **52**, 22–31.
- 29 K. Matsuo and T. Yasuda, *Chem. Commun.*, 2019, **55**, 2501–2504.
- 30 Y. Z. Shi, K. Wang, X. Li, G. L. Dai, W. Liu, K. Ke, M. Zhang, S. L. Tao, C. J. Zheng, X. M. Ou and X. M. Zhang, *Angew. Chem., Int. Ed.*, 2018, **57**, 9480–9484.
- 31 L. Hou, P. Ning, Y. Feng, Y. Ding, L. Bai, L. Li, H. Yu and X. Meng, *Anal. Chem.*, 2018, **90**, 7122–7126.
- 32 W. Pan, X. Zhang, P. Gao, N. Li and B. Tang, *Chem. Commun.*, 2019, **55**, 9645–9648.
- 33 R. Atchudan, T. N. Jebakumar Immanuel Edison, S. Perumal and Y. R. Lee, *ACS Omega*, 2018, **3**, 17590–17601.
- 34 H. Ma, Y. Ma, L. Lei, W. Yin, Y. Yang, T. Wang, P. Yin, Z. Lei, M. Yang, Y. Qin and S. Zhang, *ACS Sustainable Chem. Eng.*, 2018, **6**, 15064–15071.
- 35 H. Ma, Y. Qin, Z. Yang, M. Yang, Y. Ma, P. Yin, Y. Yang, T. Wang, Z. Lei and X. Yao, *ACS Appl. Mater. Interfaces*, 2018, **10**, 20064–20072.
- 36 H. Wang and G. Liu, *J. Mater. Chem. B*, 2018, **6**, 4029–4042.
- 37 F. Ren, P. Liu, Y. J. Shi, B. Tong, Z. Cai and Y. Dong, *Mater. Chem. Front.*, 2019, **3**, 57–63.
- 38 K. J. Wallace and J. H. Broome, *Light in Forensic Science: Issues and Applications*, 2018, vol. 17, p. 333.
- 39 A. Fruleux and A. Boudaoud, *Proc. Natl. Acad. Sci. U. S. A.*, 2019, **116**, 1940–1945.
- 40 N. L. B. Costa, C. R. Carvalho and W. R. Clarindo, *Cytologia*, 2018, **83**, 397–405.
- 41 P. Marhava, L. Hoermayer, S. Yoshida, P. Marhavý, E. Benkováet and J. Friml, *Cell*, 2019, **177**, 957–969.
- 42 N. Miyaura and A. Suzuki, *Chem. Rev.*, 1995, **95**, 2457–2483.
- 43 N. Menshutkin, *Z. Phys. Chem.*, 1890, **6**, 41–57.
- 44 X. Lv and W. Bao, *J. Org. Chem.*, 2007, **72**, 3863–3867.